

# Sub-seasonal interannual variability associated with the excess and deficit Indian winter monsoon over the Western Himalayas

A. P. Dimri

Received: 25 November 2012 / Accepted: 29 April 2013 / Published online: 8 May 2013  
© Springer-Verlag Berlin Heidelberg 2013

**Abstract** During the winter season (Dec., Jan., and Feb.; DJF) the western Himalaya (WH) receives one-third of its annual precipitation due to Indian winter monsoon (IWM). The IWM is characterized by eastward-moving synoptic weather systems called western disturbances. Seasonal interannual precipitation variability is positively correlated with monthly interannual variabilities. However, it was found that the monthly interannual variabilities differ. The interannual variability for Jan. is negatively correlated with that for Dec. and Feb. Because the entire seasonal interannual variability is in phase with the El Niño Southern Oscillation, it is interesting to investigate such contrasting behavior. Composite analysis based on extreme wet and dry seasons indicates that Dec. and Feb. precipitation variabilities have a high positive (low negative) correlation with eastern (western) equatorial Pacific warming (cooling), whereas Jan. precipitation variability exhibits negligible correlations. Seasonal mid/upper tropospheric cooling over the Himalayas enhances anomalous cyclonic circulation, which along with suppressed convection over the western equatorial Pacific, shifts the 200-hPa subtropical westerly jet southward over the Himalayas. Due to the upper tropospheric anomalous cyclonic circulation, mass transfer favors anticyclone formation at the mid/lower troposphere, which is enhanced in Jan. due to a warmer mid troposphere and hence decreases precipitation compared with Dec. and Feb. Additionally, a weakening of meridional moisture flux transport from the equatorial Indian Ocean to WH is observed in Jan. Further analysis reveals that mid-tropospheric and surface temperatures

over WH also play dominant roles, acting as local forcing where the preceding month's surface temperature controls the succeeding month's precipitation.

**Keywords** Indian winter monsoon · Sub-seasonal interannual variability · Western Himalayas

## 1 Introduction

The El Niño–Southern Oscillation (ENSO) is an important air–sea coupled system (Yasunari 1990) that plays a dominant role in defining variability over different regions of the world at various spatio-temporal scales. In the last decade, changes in El Niño patterns have been reported by many studies (Yeh et al. 2009; Kim et al. 2009; Karamuri et al. 2007, 2009). A declining relationship of ENSO with the Indian summer monsoon has been observed by various researchers (Kriplani and Kulkarni 1997; Krishnakumar et al. 1999, 2006; Kuchraski et al. 2007; Saha et al. 2012). The phase relationship of ENSO with the Indian northeast monsoon (Kriplani and Kumar 2004; Kumar et al. 2007; Yadav 2011) and the Indian winter monsoon (Laa and Lelieveld 2002; Dimri 2005, 2006; Roy 2006; Yadav et al. 2010; Dimri 2012) has been described by various researches.

Most research regarding the role of ENSO and other teleconnections has focused on summer monsoon precipitation, mainly because of its impact on a wide geographical area. However, with changing global climate patterns, it is imperative to analyze precipitation during other seasons over the Indian subcontinent. During the Indian winter (Dec., Jan., Feb.: DJF) monsoon (IWM), the Himalayan region receives precipitation due to eastward moving extratropical cyclones called western disturbances (WD)

---

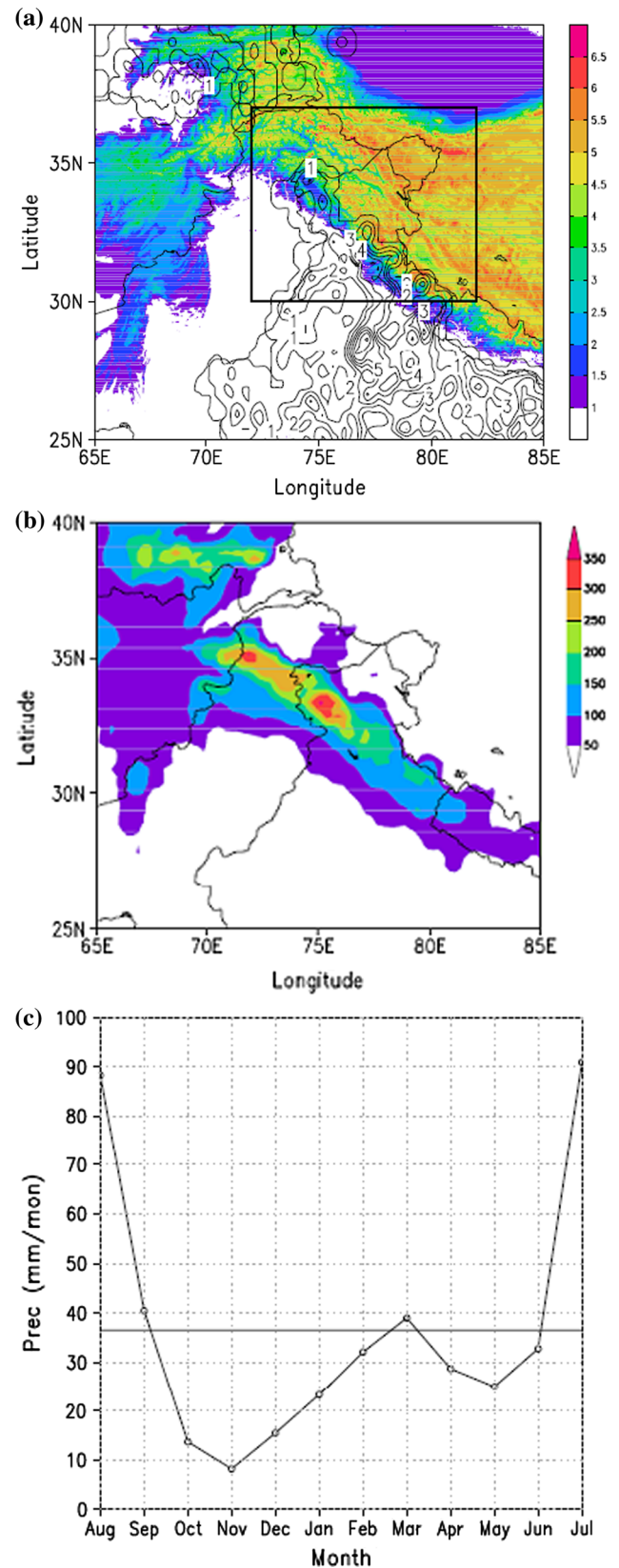
A. P. Dimri (✉)  
School of Environmental Sciences, Jawaharlal Nehru University,  
New Delhi 110067, India  
e-mail: apdimri@hotmail.com

**Fig. 1** **a** Topography ( $\times 10^{-3}$  m: shaded) and ratio of  $0.05^\circ$  grids for stations (%: contour) over the western Himalayas. The area of  $30^\circ\text{N}$ ,  $72^\circ\text{E}$  to  $37^\circ\text{N}$ ,  $82^\circ\text{E}$  is considered in the present study; **b** winter season precipitation climatology (mm/DJF) and **c** area averaged monthly precipitation climatology (mm/month); **(b)** figures are based on APHRODITE precipitation observed data reanalysis

(Dimri and Mohanty 2009). Some of these events even result in rainfall in the far northeast region of India (Pant and Rupakumar 1997). Yadav et al. (2010) and Dimri (2012) have determined the role of ENSO forcings associated with the IWM. The precipitation associated with the IWM provides crucial inputs to northern Indian rivers, glaciers, ecosystems, and habitats and is hence important to understand (Dai 1990; Lang and Barros 2004; Ueno 2005; Ueno and Aryal 2008).

However, the processes governing sub-continental scale circulation changes during the IWM over the WH have not yet been fully elucidated. The WH region includes topographic heterogeneity and land-use variability (Fig. 1a). The interplay between the WH topography/land use and winter weather makes an understanding of precipitation mechanisms complex. Additionally, most in situ observations are situated either in valley bottoms or at the windward/leeward side of ridges. There are certain limitations when making general evaluations of the WH based on these limited in situ observations (Fig. 1a). The observations pertaining to solid or liquid precipitation during winter over this region is still needed to be fully verified. Hence, very little has been determined concerning the interaction between snow cover and land surface over the WH due to the lack of information regarding initial conditions and the difficulties involved in treating complex topography in the precipitation reanalysis. Himalayan winter weather also differs considerably from that during the monsoon season, when the WDs are the main cause of snowfall over large areas. Therefore, monthly scale anomalous surface air temperatures are likely to be strongly linked to the activity of synoptic-scale disturbances, which change the area under snow cover, thus modifying the local surface heat flux in deep valleys. Also, during the IWM, it is difficult to assess precipitation events over the WH.

It is known that monthly (Dec., Jan., and Feb) interannual variabilities in precipitation are positively correlated with the corresponding seasonal (DJF) interannual variability in precipitation, but they are not in phase with each other. Jan. interannual variability is negatively correlated with Dec. and Feb. interannual variabilities. ENSO forcing has a similar behavior during the whole season (DJF), and thus the reason that the Jan. interannual variability is opposite that of Dec. and Feb. is unclear. To address this



question, the present study analyzes variability in IWM over the WH and examines the potential role of local forcings in tandem with global forcings.

## 2 Data

Precipitation records from various sources (APHRODITE: 0.25° resolution, Yatagai et al. 2009; GPCP: 2.5° resolution, Adler et al. 2003; GPCC: 1° resolution, Rudolf et al. 2005; CRU:0.5° resolution, New et al. 2000) were used to assess winter precipitation distribution over the WH. The various sets of precipitation data were used to establish how the varying spatial distribution of precipitation is captured by various analyses over the WH region. This is important, as mentioned before, because this region comprises deep valleys and high ridges, and hence the quality of initial observations is key for any further analysis. The number of stations per grid cell is available for APHRODITE (Fig. 1a) and GPCC. This information can be very useful to determine to what extent the gridded precipitation is determined from station data or is derived using interpolations between the stations. GPCP uses algorithms applied to satellite measurements to interpolate data over the land and ocean. This is important in the WH because attention to multiple meteorological elements could reveal mountain weather changes associated with the maturation of large-scale circulations (Ueno et al. 2008). Additionally, NCEP/NCAR reanalysis of large-scale fields (Kanamitsu et al. 2002) and Hadley Center sea-surface temperature data (Hadley Centre 2006) were also used to study the interannual variability over and around mid-latitude circulations and associated winter precipitation over the WH during the IWM. Long-term satellite estimates of outgoing longwave radiation (OLR) also provide important information to diagnose intraseasonal variability in climatic conditions in remote regions. Interpolated OLR data from the US National Oceanic and Atmospheric Administration (NOAA) (Liebmann and Smith 1996) were used to identify such seasonal and ground dependency. These data are distributed in 2.5° grids over monthly time intervals. Monthly OLR variability is a good indicator of cloud formations associated with precipitation. Near-surface temperature changes due to snow cover are also likely to contribute to the variation in OLR over the WH.

## 3 Results and discussion

A brief review of winter precipitation climatology is presented here. This is followed by a discussion of interannual variability with composites of wet and dry years, followed by a discussion of the linkages of the IWM with global and

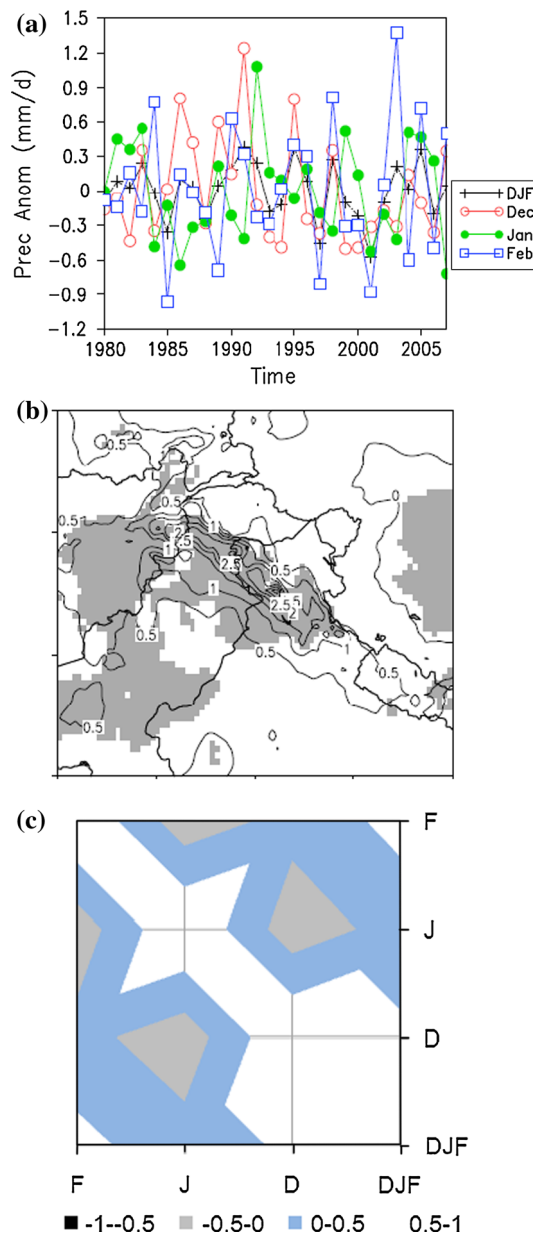


**Fig. 2** a The monthly (Dec., Jan., and Feb.) and seasonal (DJF) precipitation (mm/d) anomaly in APHRODITE observational reanalysis; b difference in 3-month (Dec., Jan., and Feb.) average wet- and dry-year composites precipitation (shaded) and region with 99% confidence level (within contour); and c correlation between seasonal (DJF) and monthly (Dec., Jan., and Feb) interannual precipitation variability

local forcings to determine the reasons for the contrasting behavior of monthly interannual variabilities.

### 3.1 Wet and dry winters over the WH

In the WH, a region from 30°N, 72°E to 37°N, 82°E (indicated by the box in Fig. 1a) was chosen for the analysis of winter precipitation and its associated interannual

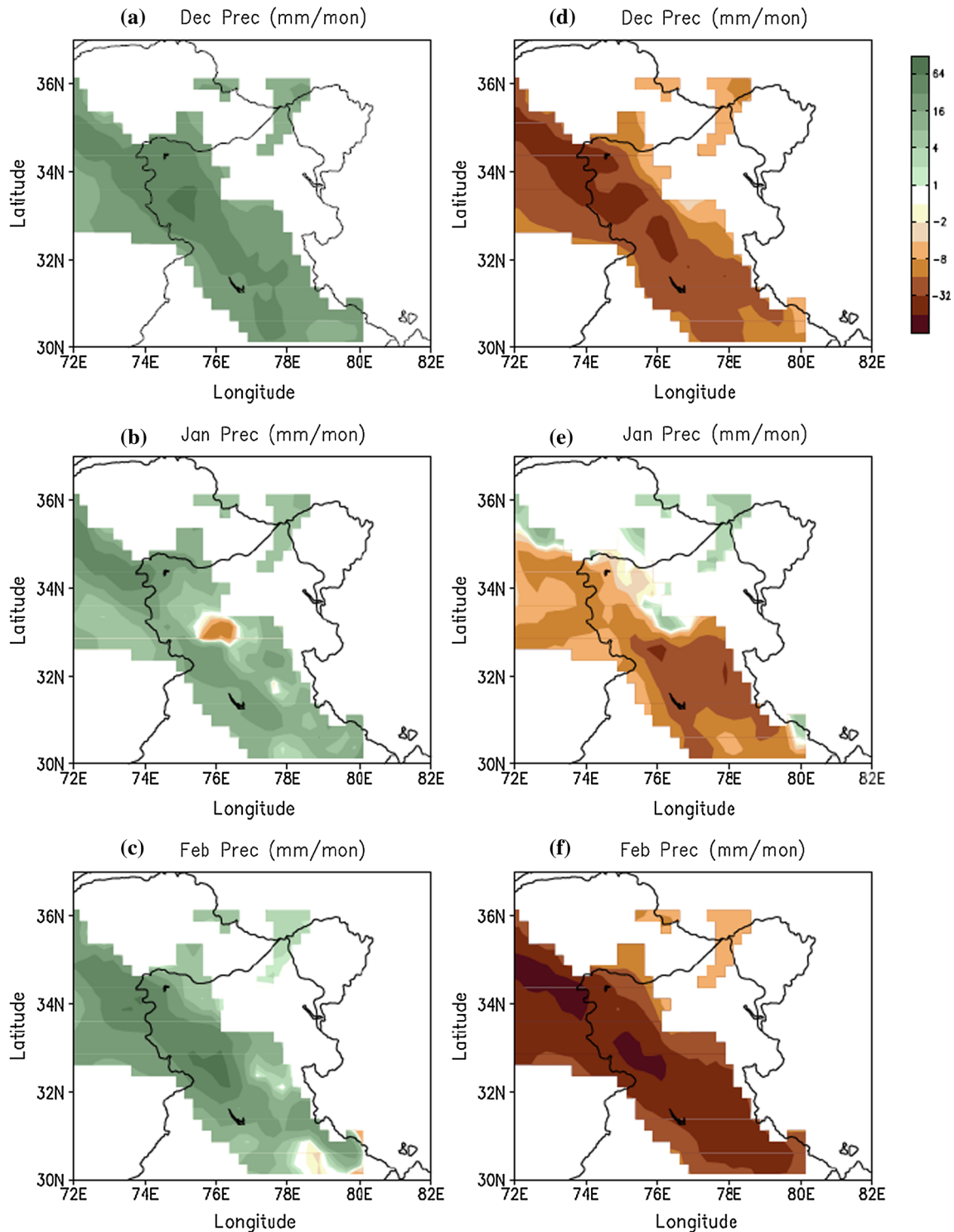


**Fig. 3** Cumulative average monthly anomalous precipitation (mm/mon) during wet composites of **a** Dec., **b** Jan., and **c** Feb and for dry composites of **d** Dec., **e** Jan., and **f** Feb. Masking with 10 mm/mon was employed

variability. This region was chosen because the area receives the highest winter precipitation and is topographically variable. Figure 1b shows the seasonal precipitation climatology based on reanalysis of APHRODITE

observations. Winter precipitation climatology is distributed across WH topography. Two zones of precipitation maxima are apparent at  $\sim 34^{\circ}\text{N}$ ,  $76^{\circ}\text{E}$  and  $\sim 35^{\circ}\text{N}$ ,  $72^{\circ}\text{E}$ . Additionally, Fig. 1c depicts the monthly climatology for

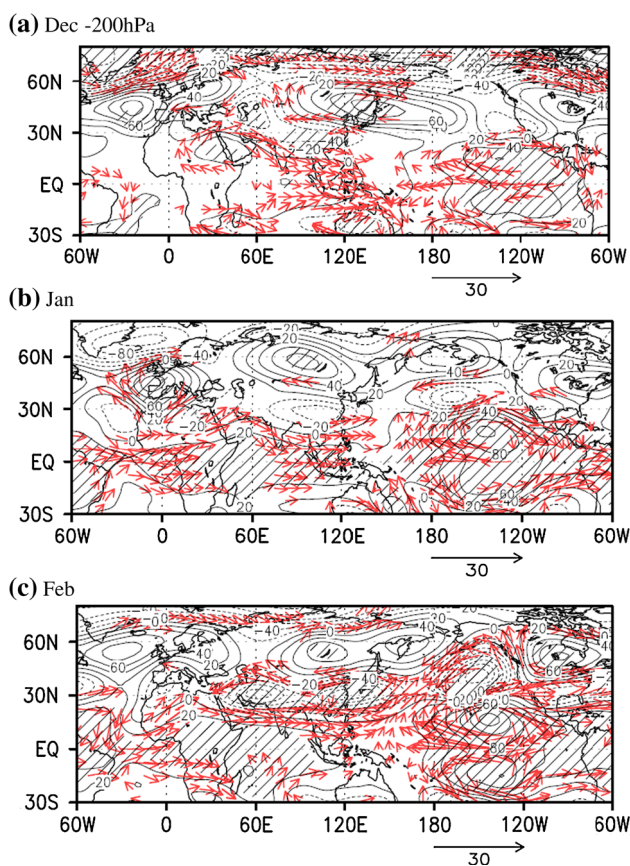


**Fig. 4** Monthly difference in (wet-dry) anomaly for 200-hPa geopotential height (hPa, contour) and wind vector ( $\text{m s}^{-1}$ , arrow) for **a** Dec., **b** Jan., and **c** Feb. The hatched region corresponds to  $\geq 95\%$ . Similarly, only winds with 95% significance and above are shown

area-averaged precipitation. Apart from a monsoonal peak in June and July, there is also significant precipitation during winter (DJF). This winter-precipitation climatology based on APHRODITE data was compared with the reanalysis of other observed data (GPCP, GPC, and CRU). Correlations  $>0.8$  were recorded between APHRODITE data and these reanalyzed data. Furthermore, the winter seasonal-to-annual precipitation ratio shows that one-third of annual precipitation is received during winter. The spatial precipitation pattern over the WH is similar for all four gridded precipitation sources. Of these four reanalyses of observed precipitation, APHRODITE reanalysis data are used here for further analysis and discussion because they have the finest spatial resolution. It should be noted that over such a region, some data may be ‘synthetic’ due to the various algorithms used while preparing the reanalysis of precipitation fields. However, this issue is beyond the scope of the present study.

Area averaged winter monthly (Dec., Jan., and Feb) and seasonal (DJF) precipitation anomalies over the WH are presented in Fig. 2a, which shows wet and dry months

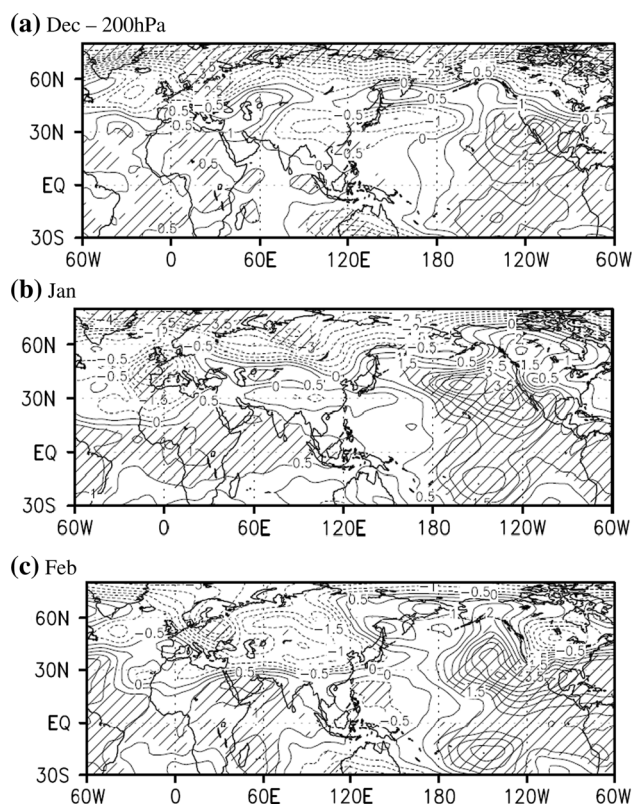


**Fig. 5** Same as Fig. 4, but for air temperature ( $^{\circ}\text{C}$ , contour)

and seasons. Based on the above and below 0.5 standard deviation extreme wet and dry seasons (DJF) were chosen (hereafter wet and dry). These were 1983, 1991, 1992, 1995, 1998, and 2005 (wet) and 1985, 1988, 1997, 2000, 2001, and 2006 (dry). Figure 2b presents the precipitation difference (shaded) between wet- and dry-year composites. Regions within the contour are significant at the 99% confidence level. This figure shows a region of significantly higher precipitation across the topography in the WH. Seasonal (DJF) interannual precipitation variability is positively correlated with individual monthly interannual precipitation variability (0.60 for Dec., 0.20 for Jan., and 0.65 for Feb; Fig. 2c). Dec. and Feb. show a higher degree of correlation than does Jan. It was found, however, that monthly anomalous interannual variabilities in the winter months (Dec., Jan., and Feb.) were negatively correlated with one another (Fig. 2c; correlations for all 12 months are presented, but discussion is limited to the winter months). Jan. interannual variability was negatively correlated with interannual variability in Dec. ( $-0.29$ ) and Feb ( $-0.30$ ). The present study addresses the reason for such behavior using a seasonal and monthly composite analysis for selected extreme precipitation years.

Initially the corresponding composite monthly anomalous precipitation distribution during wet (Fig. 3a–c) and

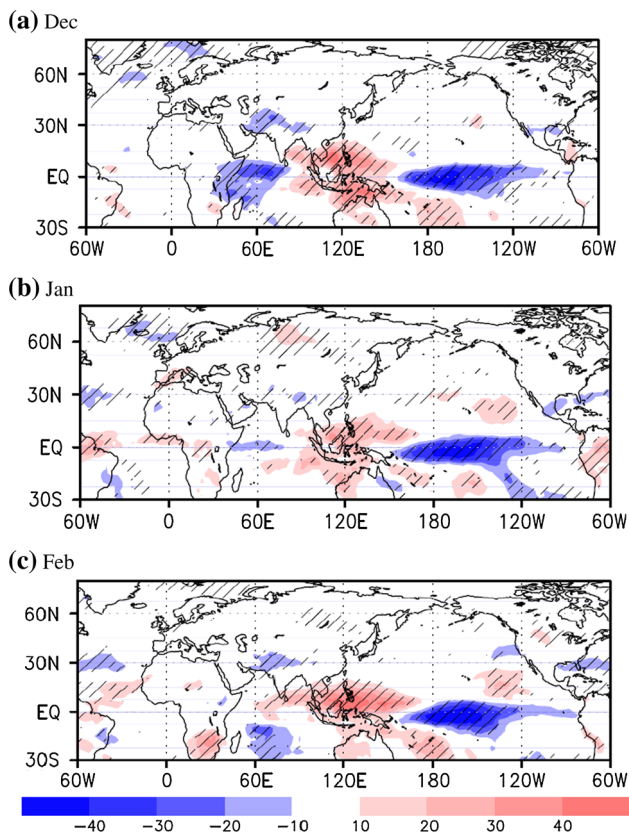


**Fig. 6** Same as Fig. 4, but for outgoing longwave radiation ( $\text{W/m}^2$ , shaded)

dry (Fig. 3d–f) years was analyzed. To remove the effect of inadequate in situ observations from the observational reanalysis, field masking with a 10-mm/month threshold was employed. This indicates that Jan. anomalous precipitation is reduced (enhanced) during wet (dry) years, Fig. 3b (Fig. 3e) than that in Dec., Fig. 3a (Fig. 3d), and Feb., Fig. 3c (Fig. 3f). The Jan. composite precipitation for wet (dry) years shows less (more) precipitation than the Dec. and Feb. values. In the case of composite precipitation for dry years, Jan. shows a relatively higher anomalous precipitation when compared with those for Dec. and Feb. Such contrasting sub-seasonal/bi-monthly behavior was studied, and a rationale for such patterns and associated variability is discussed in the following section.

### 3.2 Circulation

During excess winter significant anomalous cyclonic circulation associated with IWM exists over the Himalayas due to suppressed convection over western equatorial tropical Pacific (Kawamura 1998; Dimri 2012, 2013). To assess this dynamical role during excess and deficit IWM, Fig. 4 presents wet-minus-dry composites at 200-hPa height (contours) and wind (vector) for Dec. (Fig. 4a), Jan.

**Fig. 8** Longitude–pressure vertical cross section at  $30^\circ\text{N}$  of the anomalous meridional moisture flux ( $\text{kg/m/s}$ ) during wet ((a), (b), and (c)) and dry ((d), (e), and (f)) composites of Dec., Jan., and Feb., respectively

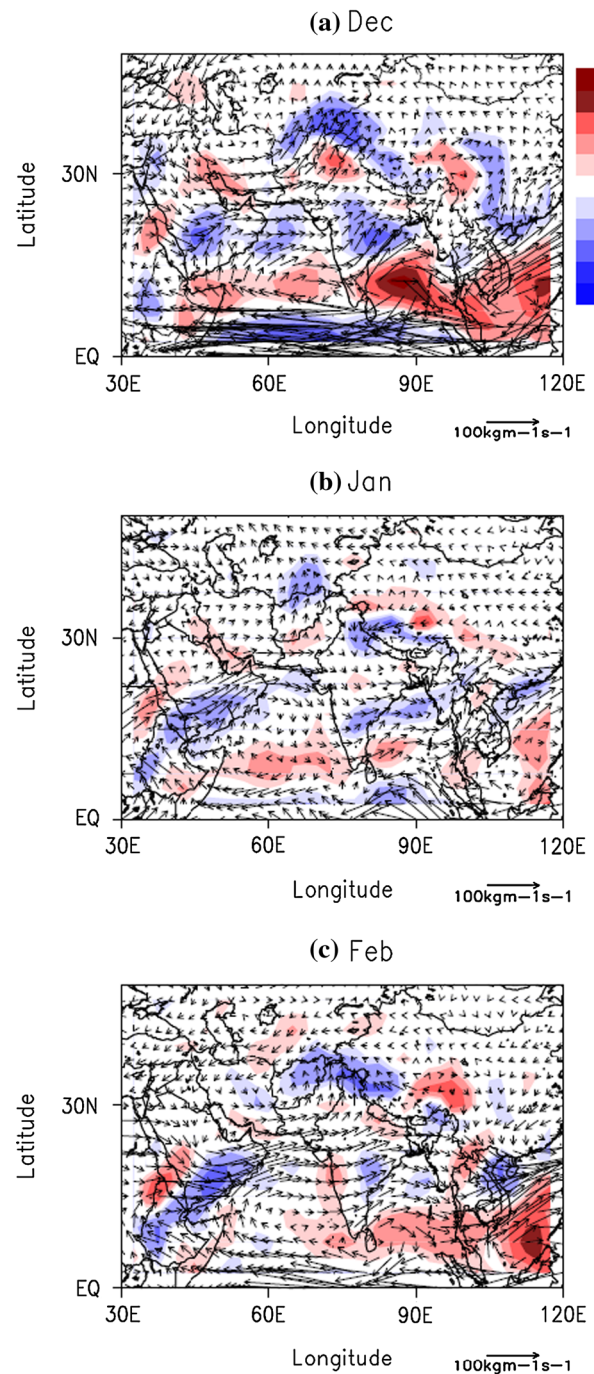
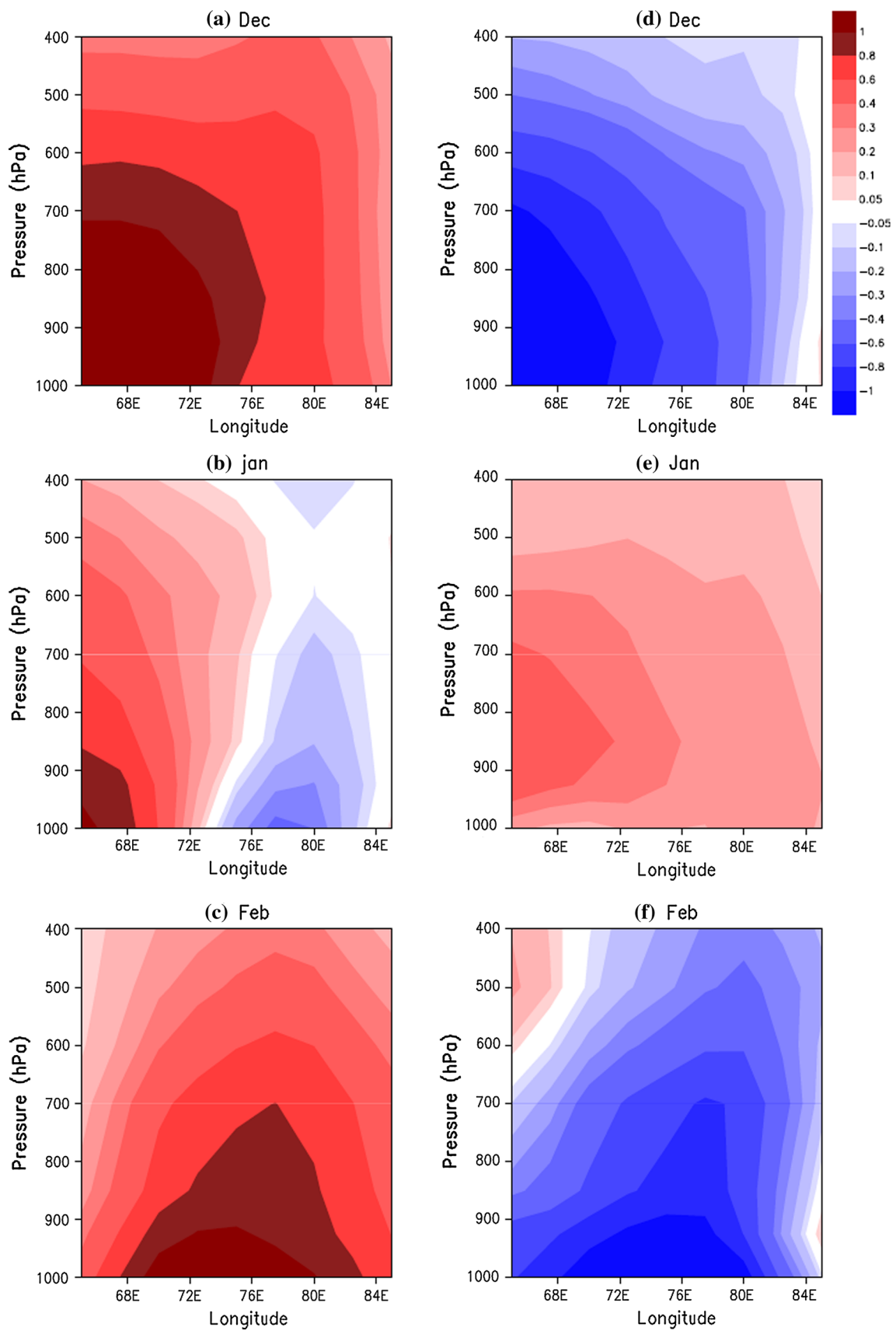


**Fig. 7** Same as Fig. 4, but for vertical integrated moisture flux (vector,  $\text{kg/m/s}$ ) and divergence (shaded,  $*1\text{e}5/\text{s}$ )

(Fig. 4b), and Feb. (Fig. 4c), respectively. The hatched region corresponds to  $\geq 95\%$  significance level. Similarly, only wind data  $\geq 95\%$  significance level is shown. Broad differences between the wet and dry monthly composites



indicate that in the upper troposphere, a significant anomalous cyclonic circulation extending up to south China Sea prevails over the Himalayas during Dec. and Feb. which weakens during Jan. and is not significant. Another anomalous anticyclonic circulation located over the Siberian region during Dec. weakens and becomes more elongated during Jan. and shifts northwards during Feb. During Jan., a well-defined anomalous anticyclonic circulation exists over the North African region in the west of the Himalayas. Corresponding wind fields suggest that over the north of the Himalayas/Tibetan Plateau, slower westerlies prevail during wet years than that during dry years. In particular, slower westerlies dominate during Dec. and Feb. than that during Jan. In the mid-troposphere, at 500 hPa, anomalous cyclonic circulation over and around the WH prevails during Dec. and Jan. (data not shown). Detailed scrutiny indicates that during Dec., an elongated significant anomalous cyclonic circulation spreads over the west of the Himalayan region and then decays during Jan. However, an anomalous anticyclonic circulation over the Caspian Sea region prevails, which strengthens during Jan. and becomes an anomalous cyclonic circulation during Feb. It was observed that during Jan the anomalous cyclonic circulation weakens over the Himalayas, in contrast to the situations during Dec. and Feb. Corresponding significant wind data indicate that winds over the equatorial Indian Ocean, which are slower westerlies during Dec., are almost neutral during Jan. and then become faster westerlies during Feb. In addition, northward propagation weakens during Jan. In the lower troposphere, at 850 hPa, stronger northwest wind propagation dominates during Dec. and Feb and becomes almost neutral during Jan. (data not shown). This propagation at the surface, arising from moisture flux transport from the equatorial Indian Ocean to the WH, strengthens the IWM during Dec. and Feb. more than during Jan.

Corresponding air-temperature conditions associated with the IWM are presented in Fig. 5. This illustrates the upper tropospheric wet-minus-dry composite air-temperature distribution. It can be clearly observed that Jan. is much warmer over the Himalayas than are Dec. and Feb during wet seasons. This anomalous warming during Jan. may be caused due to the presence of anomalous anticyclonic circulation, which in the process reduces flux exchanges from northern winter currents. This anomalous warming during Jan, may contribute to a weakening of cyclonic formation in the sub-seasonal phase. At the mid-tropospheric level (data not shown) also Jan. exhibits an anomalous warming over the Himalayan region, greater than that during Dec. and Feb. Similarly, in the lower troposphere, at 850 hPa (data not shown), significant cooling occurs over the head of the Arabian Sea and the entire Indian subcontinent during Dec. and Feb., in contrast to the relative warming during Jan.

To analyze associated convection on the global scale, Fig. 6 illustrates the anomalous OLR for wet-minus-dry-month composites. The resulting OLR distribution shows a negative OLR (strong convection) over the eastern equatorial Pacific Ocean, a positive OLR (weak convection) over the western equatorial Pacific Ocean, and a negative OLR (strong convection) over the Indian Ocean. This distribution of OLR is related to warming (cooling) of the eastern (western) equatorial Pacific Ocean linked with El Niño. During the positive phase of El Niño, enhanced warming is associated with strong convection and hence enhanced cloud cover over the eastern equatorial Pacific region, whereas suppressed convection occurs over the western equatorial Pacific region due to anomalous cooling. This suppressed convection over the western equatorial Pacific Ocean generates increased anomalous cyclonic circulation over the Himalayan region due to the Rossby

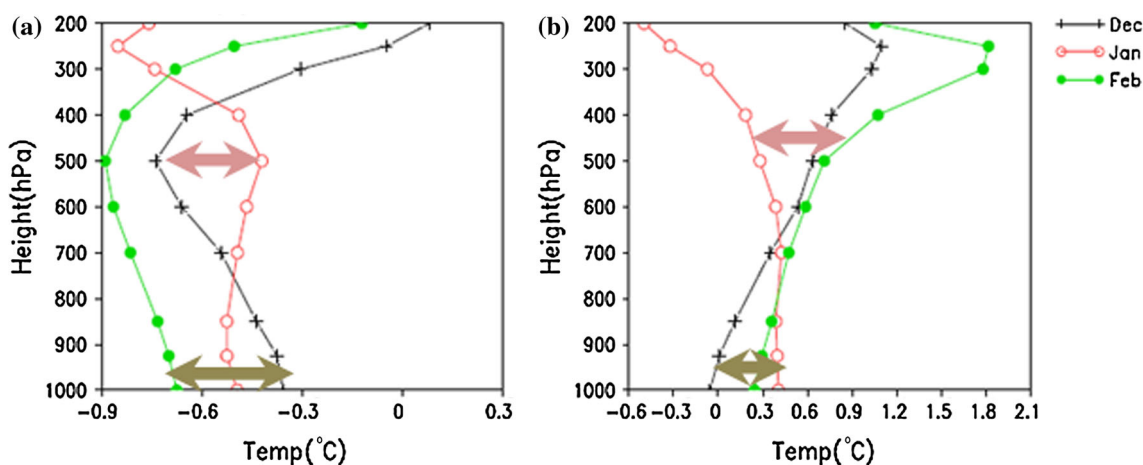


**Fig. 9** Area-averaged ( $30^{\circ}\text{N}72^{\circ}\text{E}$  to  $37^{\circ}\text{N}82^{\circ}\text{E}$ ) vertical cross-sectional distribution of anomalous air temperature ( $^{\circ}\text{C}$ ) in (a) wet and (b) dry composites for Dec. (black line), Jan. (red line), and Feb. (green line)



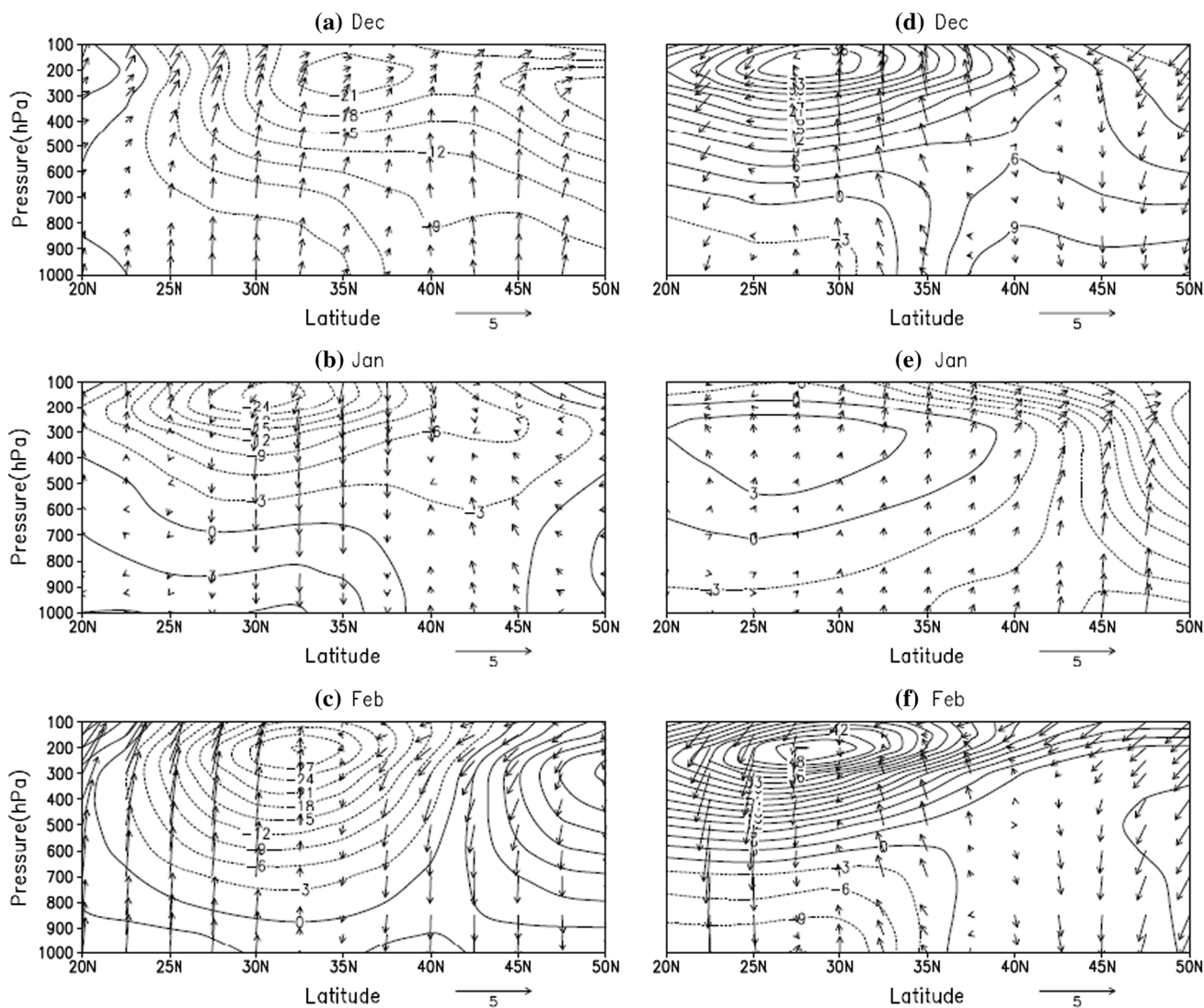


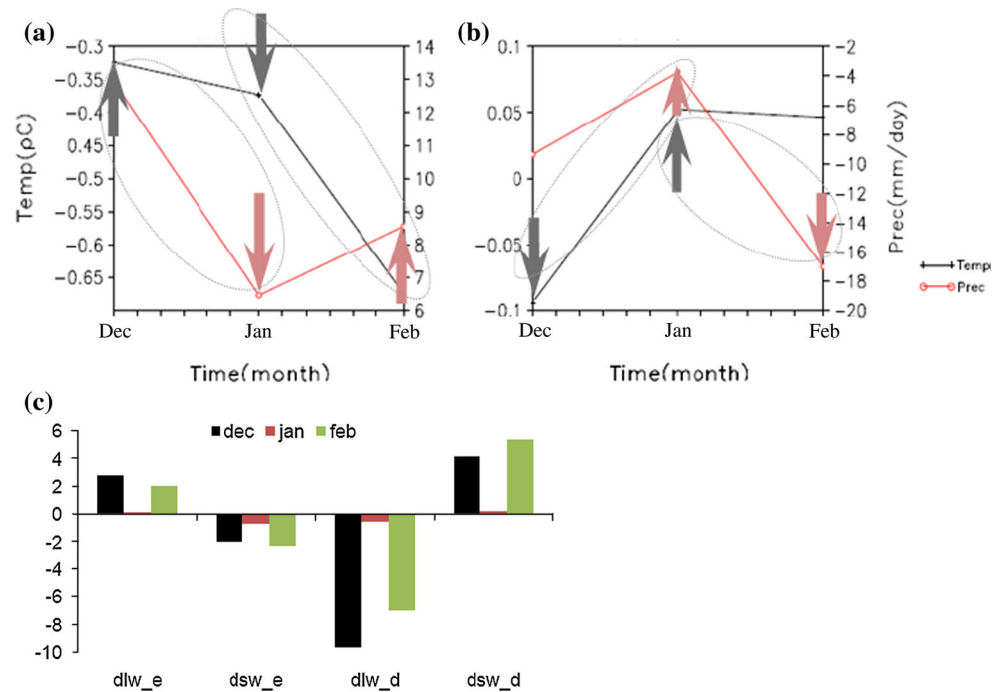
**Fig. 10** Latitude–vertical cross-sectional distribution of averaged (72°E to 82°E) geopotential height (hPa) and wind vector (m/s) in wet ((a), (b), and (c)) and dry ((d), (e), and (f)) monthly composites of Dec., Jan., and Feb. respectively

response (Kawamura 1998; Dimri 2013). Convection associated with attenuated Walker circulation over the eastern equatorial Pacific Ocean remains similar during all the 3 months, but convection is suppressed over the western equatorial Pacific Ocean, and convection over the equatorial Indian Ocean weakens more during Jan. than during Dec. and Feb. The Indian Ocean exhibits higher convection during Dec. and Feb., which does not occur during Jan. The increased convection over the Indian Ocean is mainly suppressed by low-level clouds during the IWM (Bony et al. 2000). This stronger heating during Dec. and Feb compared with Jan (around ~60–70°E) enhances Hadley circulation during Dec. and Feb. compared with Jan. (Tanaka et al. 2004), along with an attenuated Walker circulation (Kawamura 1998). This increased Hadley circulation provides a greater mass transport from the

Southern to Northern Hemisphere during Dec. and Feb. compared with Jan.

Corresponding monthly moisture fluxes (wet–dry) and divergence were analyzed to establish the repercussion of the dynamics discussed above. Figure 7 depicts the enhanced convergence over the WH associated with the IWM during Dec. (Fig. 7a), which almost becomes neutral during Jan. (Fig. 7b) and then shows higher convergence during Feb. (Fig. 7c). Stronger anomalous southwesterly moisture fluxes transport moisture from the equatorial Indian Ocean to the Himalayan region (Dimri 2007). During Jan., this flow weakens and becomes anomalously high over the Arabian Sea. To investigate this further, Fig. 8 illustrates the longitudinal–vertical cross-sectional distribution of anomalous meridional transport at 30°N during wet (Fig. 8a–c) and dry (8d–f) months. It can be

**Fig. 11** Area-averaged (30°N, 72°E to 37°N82°E) anomalous 2-m surface-air temperature (black line, °C) and anomalous precipitation (mm/d) during **a** wet and **b** dry year composites of Dec., Jan., and Feb. **c** Area-averaged anomalous downward longwave and shortwave fluxes during wet- (dlw\_e and dsw\_e) and dry-year (dlw\_d and dsw\_d) composites



clearly seen that wet conditions in Dec. and Feb. result in higher meridional moisture flux, which weakens during Jan., particularly beyond 75°E and in the lower troposphere. During dry composites, the opposite is seen.

During an El Niño phase, symmetric circulations over the equatorial Pacific Ocean, anticyclonic in the Northern Hemisphere and cyclonic in the Southern Hemisphere, start building up in Dec. and peak in Feb. The response from the IWM is similar throughout the winter. For the whole winter season (DJF), the IWM remains in phase with these compared with Jan., and the anomalous lower precipitation during Jan. is influenced by sub-seasonal/bi-monthly oscillations within the IWM. The discussion above suggests that warming/cooling of the Indian Ocean basin seems to be the dominant effect in defining sub-seasonal/bi-monthly behavior during the IWM (Fig. 6).

### 3.3 Large-scale global and local forcings

To determine large-scale global forcings, first the correlation of monthly winter precipitation over the WH with the concurrent and preceding months' sea-surface temperature (data not shown) for 28 years (1980–2007) was studied. The correlation of Dec. and Feb. monthly winter precipitation over the WH with the concurrent month's sea-surface temperature reveals similar patterns. Both were positively (negatively) correlated with the eastern (western) equatorial Pacific Ocean and the equatorial Indian Ocean sea-surface temperatures. This suggests that the eastern (western) equatorial Pacific Ocean warming (cooling) during Dec. and Feb. is in phase with the

increased precipitation over the WH. For Jan., no significant correlation exists. Rather Jan. precipitation is negatively correlated with the equatorial Indian Ocean sea-surface temperature in the preceding Dec., whereas Feb. precipitation is strongly and positively correlated with equatorial Indian and western equatorial Pacific Ocean sea-surface temperatures for Dec. and Jan. These results suggest that warming (cooling) over the eastern (western) equatorial Pacific Ocean influences Dec. and Feb. precipitation more than Jan. precipitation. The Indian Ocean warming also influences Dec. and Feb. precipitation in the opposite manner to the influence on Jan. A similar analysis using 2-m surface-air temperatures shows that Jan. precipitation is influenced more by the preceding Dec. surface-air temperature (data not shown). A correlation between Jan. precipitation and Dec. 2-m surface temperature indicates that the preceding month's cooling over the equatorial Indian Ocean and warming over the west of the WH provides conditions conducive for higher precipitation. Dec. cooling over the north of the equatorial Pacific Ocean also corresponds to higher precipitation. A similar analysis using Feb. precipitation and Jan. temperature data produced the opposite correlations. In this case the equatorial Indian Ocean warming and the western (eastern) equatorial Pacific Ocean cooling (warming) were positively and strongly correlated. This may be attributed to the fact that during the wet phase, Jan. precipitation is controlled more strongly by the Indian Ocean temperature patterns, by local forcings over the WH region, or by both, and contrasts with conditions during Dec. and Feb.

To further investigate the role of air temperature in controlling precipitation, anomalous air temperatures averaged over the WH region in wet and dry monthly composites are presented in Fig. 9a, b respectively. During the wet phase, Dec. and Feb. temperatures show cooling (warming) in the middle (upper) troposphere. This is in contrast to Jan., when warming (cooling) takes place in the middle (upper) troposphere. Jan. remains warmer (colder) in the middle (upper) troposphere than in Dec. and Feb. Also, almost similar vertical temperature distribution from surface to mid troposphere is seen during Jan. In the case of dry years, Dec. and Feb. remain warmer (colder) than Jan. from the middle to upper (lower) troposphere. In wet and dry phases, both Dec. and Feb. show similar vertical distributions of air temperature compared with Jan. With reference to Figs. 4 and 5 such distribution leads to the more warmer mid atmosphere during Jan. month. In the case of a wet year, upper tropospheric anomalous cooling induces a pressure decrease in the upper troposphere, as shown in the vertical cross section of Fig. 10a–c. This pressure drop increases the poleward pressure gradient force to the south of the cooling region, which in turn enhances the 200-hPa SWJ movement toward southern longitudes during winter. Such tropospheric cooling-induced mass change also enhances the lower tropospheric pressure, resulting in anomalous anticyclonic circulation beneath the middle/upper tropospheric cooling, as shown in Fig. 10b (Yu et al. 2004). In the case of Jan., a simultaneous middle-tropospheric warming over the WH enhances this anomalous anticyclone. To the east of this anticyclonic center, anomalous northerly winds increase over the Indian subcontinent (Fig. 4b), which signifies a weakening of winter precipitation during Jan. Such a situation also generates changes in the upward/downward winds, as seen in Fig. 10a–c. In the case of a dry year, shown in Fig. 10d–f, Jan. shows a weaker anomalous anticyclone than that during Dec. and Feb., which could result in higher precipitation during a dry-phase Jan. compared with Dec. and Feb. Prevailing wind directions in the region of 20° to 35°N are also different during Jan.

The corresponding analysis of lower tropospheric temperature differences (Fig. 9a, b) also produces very interesting results. The WH area-averaged anomalous 2-m surface-air temperatures and anomalous precipitation for wet and dry years are shown in Fig. 11a, b. These data show that if the preceding month's surface temperature increases (decreases), the succeeding month's precipitation decreases (increases). Based on such an observation, a hypothesis is proposed that the preceding month's surface forcing also affects the succeeding month's precipitation. Corresponding WH area-averaged surface (downward longwave and shortwave) fluxes are presented in Fig. 11c. This illustrates that Jan. always has anomalously low

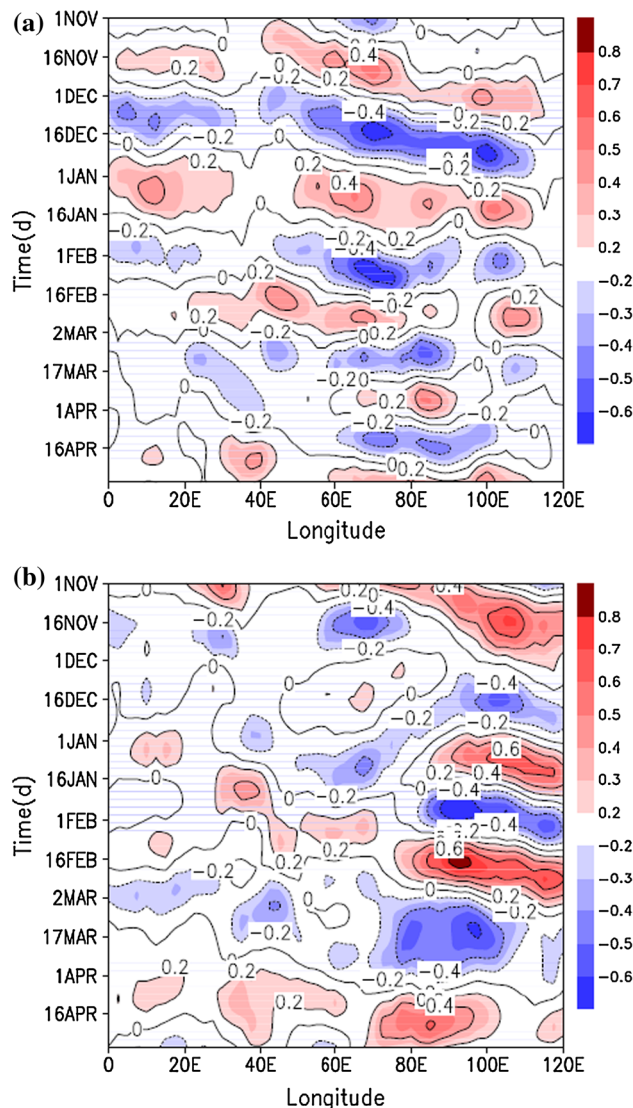


**Fig. 12** Time–longitude distribution of averaged (10°N–10°S) OLR during **a** wet- and **b** dry-year composites

fluxes, in both the wet and dry phases. This, together with the hypothesis proposed above, still needs to be studied in detail. However, it is clear that sub-seasonal/bi-monthly oscillations are seen in the IWM. To corroborate this with Indian Ocean forcing, Fig. 12 presents time–longitude distributions of averaged (10°S–10°N) OLR for wet- (Fig. 12a) and dry-phase (Fig. 12b) composites. During the wet phase, an eastward-propagating convective wave train with a phase speed of  $\sim 1^\circ$  longitude per day and a period of 30–60 days is observed. Between 1 Dec. and 1 Jan. and then again from 25 Jan. to 20 Feb., the convective system propagates eastward. This analysis corresponds to the existence of sub-seasonal/bi-monthly oscillations in the IWM. It will be examined in detail, together with the hypothesis proposed above, in a future study.

## 4 Conclusions

The impact of global and local forcings on the Indian winter monsoon has been assessed. It was found that although the interannual variability of individual months is in phase with seasonal interannual variability, the interannual variability of individual months is not in phase with other months. A positive ENSO phase corresponds to a southward positioning/shifting of the 200-hPa SWJ. The reduction in Jan. precipitation is influenced by the equatorial Indian Ocean surface temperature due to the weakening of the Hadley response during Jan., compared with Dec. and/or Feb. Additionally, comparatively greater middle-tropospheric warming during Jan. enhances the middle tropospheric anticyclone with an increased northerly wind to the east compared with during Dec. and Feb. Such sub-seasonal/bi-monthly oscillations in the IWM correspond to higher precipitation during Dec. and Feb. relative to Jan. A hypothesis has been proposed that the preceding month's surface conditions influence the succeeding month's precipitation, which will be tested in a future study.

## References

- Adler RF, Huffman GJ, Chang A, Ferraro R, Xie P, Janowiak J, Rudolf B, Schneider U, Curtis S, Bolvin D, Gruber A, Susskind J, Arkin P (2003) The version 2 global precipitation climatology project (GPCP) monthly precipitation analysis (1979–Present). *J Hydrometeorol* 4:1147–1167
- Bony S, Collins WD, Fillmore DW (2000) Indian Ocean low clouds during the winter monsoon. *J Climate* 13:2028–2043
- Dai J (1990) Climate in the Qinghai-Xizang Plateau (in Chinese). China Meteorol, Beijing
- Dimri AP (2005) The contrasting features of winter circulation during surplus and deficient precipitation over Western Himalayas. *PAGEOPH* 162(11):2215–2237
- Dimri AP (2006) Surface and upper air fields during extreme winter precipitation over Western Himalayas. *PAGEOPH* 163(8):1679–1698
- Dimri AP (2007) The transport of mass, heat and moisture over the western Himalayas during winter season. *Theoret Appl Climatol* 90(1–2):49–63
- Dimri AP (2012) Relationship between ENSO phases and northwest India winter precipitation. *Int J Climatol*. doi:10.1002/joc.3559
- Dimri AP (2013) Interannual variability of Indian winter monsoon over the Western Himalaya. *Global and Planetary Change* (accepted)
- Dimri AP, Mohanty UC (2009) Simulation of mesoscale features associated with intense western disturbances over western Himalayas. *Meteorol Appl* 16:289–308
- Hadley Centre (2006) HadiSST 1.1 global sea-ice coverage and SST (1870–present). British Atmospheric Data Centre. <http://badc.nerc.ac.uk/data/hadisst>
- Kanamitsu M, Ebisuzaki W, Woollen J, Yang S-K, Hnilo JJ, Fiorino M and Potter GL (2002) NCEP-DEO AMIP-II reanalysis (R-2). *Bull Amer Met Soc* 83:1631–1643
- Karamuri A, Behera SK, Rao SA, Weng H, Yamagata T (2007) El Niño Modoki and its possible teleconnection. *J Geophys Res* 112:C11007. doi:10.1029/2006JC003798
- Karamuri A, Tam C-Y, Lee W-J (2009) ENSO Modoki impact on the southern Hemisphere storm track activity during extended austral winter. *Geophys Res Lett* 36:L12705. doi:10.1029/2009GL038847
- Kawamura R (1998) A possible mechanism of the Asian summer monsoon–ENSO coupling. *J Met Soc Jap* 76(6):1009–1027
- Kim H-M, Webster PJ, Curry JA (2009) Impact of shifting patterns of Pacific Ocean warming on North Atlantic equatorial cyclones. *Science* 325:77–80
- Kripalani RH, Kumar P (2004) Northeast monsoon rainfall variability over south peninsular India vis-à-vis Indian Ocean dipole mode. *Int J Clim* 24:1267–1282
- Kriplani RH, Kulkarni A (1997) Climatic impact of El Niño/La Niña on the Indian monsoon: a new perspective. *Weather* 52:39–46
- Krishnakumar K, Rajagopalan B, Cane MA (1999) On the weakening relationship between in Indian monsoon and ENSO. *Science* 284:2156–2159
- Krishnakumar K, Rajagopalan B, Hoerling M, Bates G, Cane MA (2006) Unraveling mystery of Indian monsoon failure during El Niño. *Science* 314:115–119
- Kucharski F, Bracco A, Yoo JH, Molteni F (2007) Low-frequency variability of the Indian monsoon–ENSO relationship and the equatorial Atlantic: the “weakening” of the 1980s and 1990s. *J Clim* 20:4255–4265
- Kumar P, Rupakumar K, Rajeevan M, Sahai AK (2007) On the recent strengthening of the relationship between ENSO and northeast monsoon rainfall over South Asia. *Clim Dyn* 28:649–660
- Laat ATJ and Lelieveld J (2002) Interannual variability of the Indian winter monsoon circulation and consequences for pollution levels. *J Geophys Res* 107, D24, 4739. doi:10.1029/2001JD001483
- Lang T, Barros AP (2004) Winter storm in the central Himalayas. *J Meteorol Soc Jpn* 82:829–844
- Liebmann B, Smith CA (1996) Description of complete (interpolated) outgoing longwave radiation dataset. *Bull Amer Meteorol Soc* 77:1275–1277
- New MG, Hulme M, Jones PD (2000) Representing twentieth century space–time climate variability, Part II. Development of a 1901–96 monthly grid of terrestrial surface climate. *J Climate* 13:2217–2238
- Pant GB, Rupakumar K (1997) *Climates of South Asia*. Wiley, New York
- Roy SS (2006) The impacts of ENSO, PDO and local SST on winter precipitation in India. *Phys Geogr* 27(5):464–474
- Rudolf B, Beck C, Grieser J and Schneider U (2005) Global precipitation analysis products. Global precipitation climatology centre (GPCC), DWD, Internet publication 1–8
- Saha SK, Haldar S, Krishnakumar K, Goswami BN (2012) Pre-onset land surface processes and ‘internal’ interannual variabilities of the Indian summer monsoon. *Clim Dyn* 36:2077–2089
- Tanaka HL, Ishizaki N, Kitoh A (2004) Trend and interannual variability of Walker, monsoon and Hadley circulations defined by velocity potential in the upper troposphere. *Tellus* 56A:250–269
- Ueno K (2005) Synoptic conditions causing nonmonsoon snowfalls in the Tibetan Plateau. *Geophys Res Lett* 32:L01811. doi:10.1029/2004GL021421
- Ueno K, Aryal R (2008) Impact of equatorial convective activity on monthly temperature variability during nonmonsoon season in the Nepal Himalayas. *J Geophys Res* 113:D18112. doi:10.1029/2007JD009524
- Ueno K, Toyotsu K, Bertolani L, Tartari G (2008) Stepwise onset of monsoon weather observed in the Nepal Himalayas. *Mon Wea Rev* 136:2507–2522

- Yadav RK (2011) Why is ENSO influencing Indian northeast monsoon in the recent decades? *Int J Clim*. doi:[10.1002/joc.2430](https://doi.org/10.1002/joc.2430)
- Yadav RK, Yoo JH, Kucharski F, Abid MA (2010) Why is ENSO influencing northwest India winter precipitation in recent decades? *J Clim* 23:1979–1993
- Yasunari T (1990) Impact of Indian monsoon on coupled atmosphere/ocean system in the equatorial pacific. *Meteoro Atmos Phys* 90(1):35–57
- Yatagai A, Arakawa O, Kamiguchi K, Kawamoto H (2009) A 44-year daily gridded precipitation dataset for Asia based on a dense network of rain gauges. *SOLA* 5:137–140
- Yeh SW, Kug JS, Dewitte B, Kwon MH, Kirtman B, Jin FF (2009) El Niño in a changing climate. *Nature* 461:511–514
- Yu R, Wang B, Zhou T (2004) Tropospheric cooling and summer monsoon weakening trend over east Asia. *Geophys Res Lett* 31:L22212. doi:[10.1029/2004GL021270](https://doi.org/10.1029/2004GL021270)